CrystEngComm

Accepted Manuscript

ROYAL SOCIETY OF CHEMISTRY

www.rsc.org/crystengcomm

ARTICLE TYPE www. rsc.org/xxxxxx | XXXXXXXX

Metal enhanced $Ge_{1-x}Sn_x$ alloy film growth on glass substrates using biaxial CaF_2 buffer layer

J. K. Dash,*[a] L. Chen,[a] T. -M. Lu,[a] G. -C. Wang,[a] L. H. Zhang,[b] and K. Kisslinger [b]

Received Xth XXXXXXXXXX 20XX, Accepted Xth XXXXXXXXX 20XX
First published on the web Xth XXXXXXXXXX 200X
DOI: 10.1039/b000000x

$Ge_{1-x}Sn_x$ alloyed films were grown on glass substrates by sequential physical vapor deposition of a biaxial CaF_2 buffer layer and a Sn heteroepitaxial layer at room temperature, followed by a Ge layer grown at low temperatures (200 - 350 °C). The predeposited Sn on the CaF_2 layer enhances the Ge diffusion and crystallization. The Sn substitutes into the Ge lattice to form a biaxial $Ge_{1-x}Sn_x$ alloyed film. The epitaxy relationships were obtained from x-ray pole figures from the samples with $Ge_{1-x}Sn_x\langle\bar{1}01\rangle \parallel CaF_2\langle\bar{1}01\rangle$ and $Ge_{1-x}Sn_x\langle\bar{1}10\rangle \parallel CaF_2\langle\bar{1}10\rangle$. The crystallization and biaxial texture formation start at about 200 °C with the best biaxial $Ge_{1-x}Sn_x$ film grown at about 300 °C, which is 100 °C lower than the growth temperature of biaxial pure Ge film without Sn on the CaF_2/glass substrate.The microstructure, texture and Sn concentration of the $Ge_{1-x}Sn_x$ films were characterized by x-ray diffraction, x-ray pole figure analysis, and transmission electron microscopy. The spatial chemical composition of Sn in $Ge_{1-x}Sn_x$ was measured by energy dispersive x-ray spectroscopy and was found nearly uniform throughout the thickness of the alloyed film. Raman spectra shows shifts of Ge-Ge, Ge-Sn, and Sn-Sn vibration modes due to the percentage change of substitutional Sn in Ge as a function of growth temperature. This growth method is an alternative cost effective way to grow biaxial semiconductor films on amorphous substrates.

1 Introduction

The $Ge_{1-x}Sn_x$ alloy film is an attractive candidate for silicon based optoelectronic devices with active Ge layers. Ge has an indirect bandgap of 0.67 eV at room temperature [1] and Sn as a metal has a 0 eV bandgap. $Ge_{1-x}Sn_x$ alloy may bridge the need of small bandgap materials. Previous experimental work has shown the optical energy gap of Ge can be tuned from 0.679 eV to 0.473 eV by varying the Sn concentration x ranging from 0.02 to 0.14 in $Ge_{1-x}Sn_x$ alloy films. [2] In addition, the observed indirect to direct bandgap transition occurs for x ranging from 0.10 to 0.13. Besides the potential application in optoelectronics, Ge is a favored candidate for channel material used in the complementary metal oxide semiconductor. This is because of Ge's high electron mobility plus that the strain state of $Ge_{1-x}Sn_x$ can be adjusted by using a virtual substrate such as a Ge buffer layer on Si single crystal substrate. [1] These potential applications have attracted intense interest in the synthesis of epitaxial $Ge_{1-x}Sn_x$ films on single crystal substrates.

The challenges to grow single phase $Ge_{1-x}Sn_x$ include large lattice mismatch ($\sim$ 15 %) between alpha Sn (0.6489 nm, grey tin) and Ge (0.5657 nm), severe Sn segregation at temperatures higher than 140 °C, and low Sn solid solubility (about 1 %) in Ge. This implies that to grow $Ge_{1-x}Sn_x$ film with a wide range of x, one possible way is to use non-equilibrium growth conditions. Researchers have grown $Ge_{1-x}Sn_x$ films on single crystal substrates of Si(100) or Ge(100) using molecular beam epitaxy [3–6], magnetron sputtering [7], or chemical vapor deposition [8,9]. When the $Ge_{1-x}Sn_x$ was grown on Si(100) (Si lattice constant 0.5431 nm at 300 K), a virtual substrate or buffer layer of Ge was used to reduce the lattice mismatch between $Ge_{1-x}Sn_x$ and Si(100) instead of growing $Ge_{1-x}Sn_x$ directly on Si(100). [5,10,11] Various properties of these $Ge_{1-x}Sn_x$ films including their optical properties [4], optoelectronic properties [5], thermal stability [10,12], composition, and strain [10] on single crystal substrates have been studied.

In this work we report a new way to grow biaxial $Ge_{1-x}Sn_x(111)$ alloy film with a few percent Sn on a glass substrate instead of a single crystal substrate at temperatures below the Ge crystallization temperature of over 400 °C. The approach was to first grow a biaxial CaF_2 buffer layer on a glass substrate before adding a Sn layer on the CaF_2 buffer layer, both at room temperature. The Ge was then deposited on the Sn layer at an elevated temperature ranging from 200 °C to 350 °C and then annealed at that growth temperature in-situ for one hour. A schematic representing the growth sequence of layers is shown in Fig. 1(a). There are several advantages in this approach: (1) The biaxial $CaF_2(111)$

[a] *Department of Physics, Applied Physics and Astronomy, Rensselaer Polytechnic Institute, 110 8th Street, Troy, New York 12180, USA*
**E-mail: jatiskumar@gmail.com, dashj@rpi.edu*

[b] *Brookhaven National Lab, Center for Functional Nanomaterials Bldg. 735, P.O. Box 5000, Upton, New York 11973*

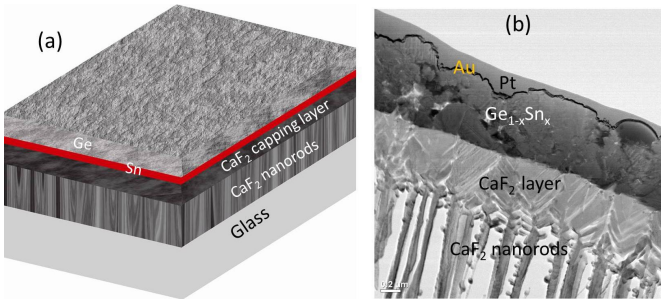

Fig. 1 A schematic of Ge / Sn / CaF_2 buffer layer (consisting of normal incident deposited capping layer and oblique angle incident deposited nanorods)/glass substrate. The schematic is not to scale. (b) TEM cross section image of $Ge_{1-x}Sn_x$ / CaF_2(capping layer + NR) / glass grown and annealed at 300 °C. The Ge and Sn form an alloy film on CaF_2.

vertical nanorods and the capping layer can be grown in sequence under oblique angle deposition and normal incidence deposition, respectively on a glass substrate at room temperature.[13,14] (2) The Sn enhances Ge diffusion, thus a compositional uniform $Ge_{1-x}Sn_x$ (111) alloy film can be formed at low temperatures. (3) For the few percent Sn concentrations that we studied, there is no obvious Sn segregation on the surface of $Ge_{1-x}Sn_x$(111) alloy film.

The structure and biaxial texture of $Ge_{1-x}Sn_x$(111) alloy films were characterized by x-ray diffraction (XRD) and x-ray pole figure analysis. Microstructures and composition profiles of the film grown at 300 °C were studied by transmission electron microscopy (TEM), selective area electron diffraction, high resolution imaging, and energy dispersive x-ray spectroscopy (EDS). The vibrational property was studied by Raman scattering. Surface morphology was imaged by atomic force microscopy (AFM).

2 Experimental

The CaF_2 molecules were evaporated from a heated W filament boat that housed CaF_2 crystal pellets (Alfa Aesar, 99.9 % purity). The CaF_2 nanorod (NR) films of thickness $\sim$ 1 μm were grown on glass substrates (Corning 2947) without intentional heating by oblique angle vapor deposition technique with a deposition angle of $\sim 70^\circ$ with respect to the surface normal in a high vacuum chamber with a base pressure of 3.1×10^{-7} Torr. The deposited film consisted of vertically aligned NR and had a biaxial texture.[13,14] A $\sim$ 500 nm thick CaF_2 capping layer was then grown on this NR film under normal incident vapor deposition. The details of this deposition procedure have been described elsewhere.[13,14] These CaF_2 (Capping layer + NR) / glass samples were used as the substrates for further Sn and Ge depositions in another vacuum chamber. The sample was first loaded into a sample holder that was equipped with an indirect substrate heater inside an ultra-high vacuum (UHV) chamber with a base pressure of $\sim$ 6.5×10^{-9} Torr. The chamber had two evaporation sources, Ge (99.9 % purity) and beta Sn (99.99 % purity), each heated in its own alumina-coated W basket. The distance between the sources and the substrate was $\sim$ 25 cm and the flux was incident near normal to the substrate. An approximately 75 nm thick Sn film was grown on a CaF_2/glass substrate at room temperature (RT) with no intentional substrate heating. The substrate reached $\sim$ 30 °C as a result of heat radiated from the heated Sn source during Sn deposition. The Sn / CaF_2 / glass substrate was then heated to the growth temperature of Ge by a pancake W lament fixed underneath the substrate holder. Then a Ge film of $\sim$ 500 nm thick was deposited on the $\sim$ 75 nm Sn/CaF_2/glass at various growth temperatures: room temperature, 200, 250, 300 and 350 °C. In the case of room temperature deposition (i.e. no intentional substrate heating) the substrate temperature rose to $\sim$ 60 °C from the heated Ge source during Ge deposition. The substrate temperature was measured by a type K thermocouple attached to the sample surface. The temperature reading is within $\pm$ 5 °C of the target temperature.

Both Ge and Sn films were grown at a constant rate of 0.38 nm/sec monitored by a quartz crystal microbalance (QCM) placed near the substrate in the vacuum chamber. All multilayer samples presented in this work were grown using the calibrated deposition rate from the sample imaged by TEM. XRD theta-2theta (θ-2θ) scans (PanAlytical XPert Pro) were performed with a divergent beam of wavelength of 1.5405 $\AA$ and a line detector with a step size of 0.013° to characterize the lattice constant and average grain size of the $Ge_{1-x}Sn_x$ alloy film. X-ray pole figures for $Ge_{1-x}Sn_x$ alloy films were collected using the same diffractometer to characterize the crystal texture orientation of $Ge_{1-x}Sn_x$ films grown at different growth and annealing temperatures. Raman spectra were collected using Witec Alpha 300 confocal Raman microscopy with a laser wavelength of 532.1 nm, and a 100× objective lens that provides a spot size of 0.7 μm (= 1.22 wavelength/numerical aperture of 0.9 for the 100× objective lens). The spectral resolution and step size used in Raman scattering were both 0.02 cm^{-1}. The laser power used for all measurements of the Raman spectra was 17 mW. The AFM images of surface morphology were scanned in contact mode using an AFM tip with a force constant of 2 N/m.

The Ge/Sn/CaF_2(capping layer + NR)/glass sample is schematically shown in Fig. 1(a). A TEM cross-section view of the sample grown and annealed for one hour at 300 °C is shown in Fig. 1(b). A uniform $Ge_{1-x}Sn_x$ alloy film is observed; there are no separate Ge and Sn layers as shown in the layer growth sequence in Fig. 1(a). An ultrathin Au layer (dark contour boarders between Pt and GeSn alloy film) was

deposited on the sample surface to make the sample conductive for focused ion beam (FIB)/ scanning electron microscopy (SEM). A sacrificial Pt layer was deposited on the surface of the Au layer for the FIB process. The sample was then thinned down by FIB milling using energetic gallium ions. The thinned sample was mounted on a liquid nitrogen cooled sample stage to minimize the samples mechanical drifting. A 200 keV energy electron beam was used in the TEM (JEOL 2100 F) for bright field images, high resolution images and electron diffraction patterns. The image shown in Fig. 1(b) indicates that the combined $Ge_{1-x}Sn_x$ alloy film thickness is about 530 $\pm$ 80 nm.

3 Results

3.1 X-ray diffraction

3.1.1 *$Ge_{1-x}Sn_x$ alloy films grown on Sn(100)/ CaF_2(111)/ glass at various growth temperatures and annealed at the same temperature after growth:*

Figure 2 shows x-ray θ *vs.* 2θ spectra from the film of amorphous Ge/Sn/CaF_2 (Capping layer + NR) / glass grown at room temperature, as well as films grown at 200, 250, 300, and 350 °C followed by one hour annealing at the same growth temperature. The one hour post annealing increases the x-ray peak intensity of the $Ge_{1-x}Sn_x$ film relative to that without the post annealing. This is due to the fact that Sn increases Ge diffusion and enhances the crystallization of $Ge_{1-x}Sn_x$ alloy film. For comparison, a pure Ge film grown at 300 °C without Sn followed by 1 hour annealing at the same growth temperature is also shown as the bottom curve in Fig. 2. All peak heights were normalized relative to the CaF_2 peak height that is set to one. The spectrum of the sample grown at room temperature shows that the most dominant peaks are CaF_2(111) at 28.30° and beta Sn(200) at 30.60°.

The beta Sn has a tetragonal structure with lattice constants a = b = 0.583 nm and c = 0.318 nm. The single Sn(200) peak shown in the θ *vs.* 2θ spectrum and x-ray pole figure indicate that the Sn was epitaxially grown on CaF_2(111) at room temperature. There is no peak from Ge because the film grown at room temperature is mainly amorphous. Three low intensity and broad peaks that neither correspond to pure Ge crystalline film nor pure Sn crystalline film show up at 26.20°, 43.60° and 51.85°. These peaks are identified as $Ge_{1-x}Sn_x$ alloy peaks of $Ge_{1-x}Sn_x$(111), $Ge_{1-x}Sn_x$(220) and $Ge_{1-x}Sn_x$(311), respectively. As the growth and annealing temperatures increased, the CaF_2(111) peak at 28.30° persisted to 350 °C. The Sn(200) peak at 30.60° also survived up to 350 °C although the intensity decreased dramatically relative to that of CaF_2 peak. The broad $Ge_{1-x}Sn_x$ alloy peaks observed at 26.20°, 43.60° and 51.85° for the film grown at room temperature gradually shifted to higher values of 2θ as the growth temperature increased. For examples the room temperature $Ge_{1-x}Sn_x$(111) peak at 26.20° shifted to 26.80°, 27.05°, 27.12° and 27.15° when the growth temperatures were 200, 250, 300, and 350 °C, respectively. These peaks have much higher intensities compared with the peak at 26.20° from the sample grown at room temperature and then annealed at higher temperatures (not shown here). This higher peak intensity implies that more crystallites were formed. The peak intensity of the $Ge_{1-x}Sn_x$(111) film increases and the peak position shifts toward higher 2θ angles as the growth temperature increases. However, the peak position of 27.15° from the $Ge_{1-x}Sn_x$(111) film grown at the highest growth temperature of 350 °C still did not reach the peak position of 27.28° for a pure Ge(111) film. This implies the film was not pure Ge. The observed change in the 2θ angle is attributed to variation in Sn concentration.

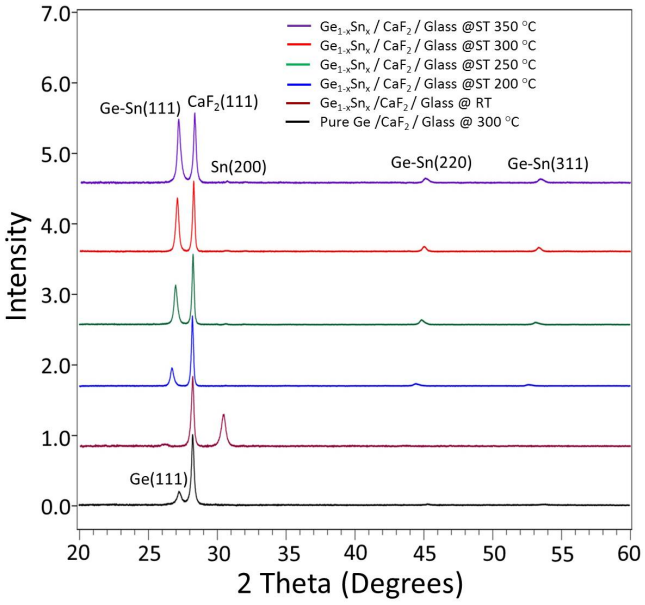

Fig. 2 X-ray θ *vs.* 2θ spectra from pure Ge / CaF_2(capping layer + NR) / glass grown at near room temperature ($\sim$ 60 °C) and no annealing (second curve from the bottom), $Ge_{1-x}Sn_x$ / CaF_2 (capping layer + NR) / glass samples grown at 200, 250, 300 and 350 °C and annealed for one hour. A pure Ge / CaF_2(capping layer + NR) / glass grown at 300 °C and annealed for one hour is shown (bottom curve).

3.1.2 *Lattice constants of $Ge_{1-x}Sn_x$ films:*

From the Bragg peak position of the alloy film, the lattice constant of the $Ge_{1-x}Sn_x$ film can be calculated. The lattice constants of $Ge_{1-x}Sn_x$(111) alloy films as a function of growth and annealing temperatures are plotted in Figure 3. The decreasing values are 0.5880, 0.5751, 0.5702, 0.5688, and 0.5682 nm for films grown at room temperature, 200, 250, 300, and 350 °C,

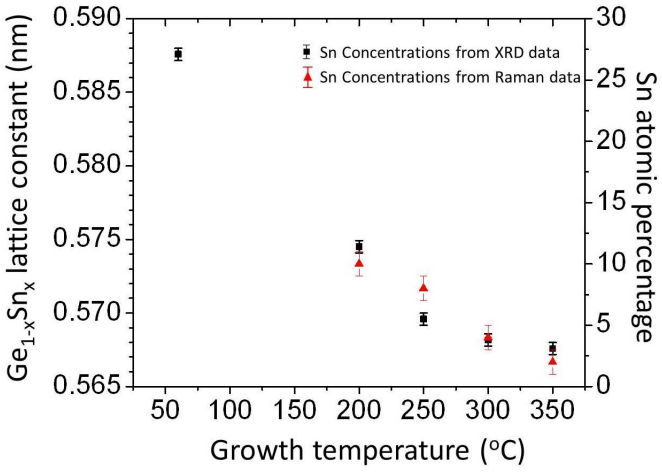

Fig. 3 Lattice constant of $Ge_{1-x}Sn_x$ film measured from XRD and Sn atomic percentage *vs.* growth temperature (black squares). The red triangles are Sn percentage obtained from the Raman Ge-Sn peak shift

respectively. As a reference, the pure Ge lattice constant is 0.5657 nm. The lattice constant of $Ge_{1-x}Sn_x$ alloy film depends on the percentage x of Sn in the film. Researchers have determined the lattice constant and corresponding Sn percentage from x-ray diffraction[7], Rutherford backscattered spectroscopy (RBS)[3,9], optical energy gap[2], and the first-principles density functional theory.[15] The RBS results show that the amount of Sn in Ge lattice sites is above 90 % substitutional in the $Ge_{1-x}Sn_x$ film.[3] Because the Sn atom is larger than the Ge atom, the original Ge lattice constant increases depending on the increased amount of substitutional Sn. By comparing our measured lattice constants from x-ray diffraction with the literature calibration curve of lattice constant *vs.* Sn concentration[3], we can estimate the concentration of Sn. The concentration decreased from 27.1 % in the sample grown at room temperature to 11.4, 5.45, 3.8, and 3.1 % (all with ± 0.5 % uncertainty) in the samples grown and annealed at 200, 250, 300 and 350 °C, respectively. See Fig. 3. This decreasing Sn percentage implies that the amount of available Sn decreases as the growth temperature increases. This is due to the relatively low melting point of Sn (232 °C): at growth temperatures higher than 232 °C some Sn had evaporated from the sample surface before the Ge deposition. The high Sn concentration determined from the x-ray peak position (lattice constant) of the $Ge_{1-x}Sn_x$ film grown at room temperature is because the major part of the deposited Ge film is still amorphous and has not participated in the alloying process. The Ge that has been alloyed with Sn formed small size, Sn rich $Ge_{1-x}Sn_x$ alloy crystallites. The lattice mismatch between CaF_2 and $Ge_{1-x}Sn_x$ alloy film grown at 300 °C is $\sim$ 4 %.

3.1.3 ***Average crystalline sizes of $Ge_{1-x}Sn_x$ films in the vertical direction:*** From the full-width-at-half-maximum (FWHM) of intensity profiles of $CaF_2(111)$, Sn(111) and $Ge_{1-x}Sn_x(111)$ peaks, the lower limit of the average crystalline grain sizes of CaF_2, Sn and $Ge_{1-x}Sn_x$ in the normal direction of samples were calculated using Debye-Scherrers formula. That is, the average crystalline size = $k\lambda/(\beta cos\theta)$, where k is a shape factor of about 0.9, λ is the wavelength of the x-ray, β is the FWHM, and θ is the Bragg angle. The $Ge_{1-x}Sn_x$ crystalline size increases from about 9.5 nm at room temperature to $\sim$ 50, $\sim$ 55, $\sim$ 62, and $\sim$ 63 nm as the growth temperature increases to 200, 250, 300 and 350 °C, respectively. The Sn crystallite size decreases from over 50 nm to less than 10 nm in the similar temperature range. This implies that Sn is incorporated into the Ge lattice substitutionally[15] and forms $Ge_{1-x}Sn_x$ alloy crystallites. Its crystallites grow in size whereas the amount of Sn crystallites decreases as the growth and annealing temperature increases. The grain size of $CaF_2(111)$ stays relatively constant at about 64 nm implying stable CaF_2 grains in the range of the growth temperature.

3.2 X-ray pole figures of biaxial $Ge_{1-x}Sn_x$, CaF_2, and Ge films

The XRD results show that the out-of-plane orientation of both CaF_2 and $Ge_{1-x}Sn_x$ films are [111]. X-ray pole figures of the $CaF_2\{111\}$ buffer layer grown at room temperature and $Ge_{1-x}Sn_x\{111\}$ grown at various temperatures were collected and analyzed. Figures 4(a) and 4(c), respectively, show pole figures of $CaF_2\{111\}$ grown at room temperature and $Ge_{1-x}Sn_x\{111\}$ grown at 300 °C and then annealed at the same temperature for one hour. The $Ge_{1-x}Sn_x\{111\}$ main poles have three-fold symmetry, as do the main poles of $CaF_2\{111\}$. The epitaxy relationships are obtained from the pole figures of $Ge_{1-x}Sn_x\langle\bar{1}01\rangle \parallel CaF_2\langle\bar{1}01\rangle$ and $Ge_{1-x}Sn_x\langle\bar{1}10\rangle \parallel CaF_2\langle\bar{1}10\rangle$. For a comparison, the pole figure of Ge{111} grown at 300 °C without Sn and annealed for 1 hour is shown in Fig. 4(b). The poles are not obvious as compared with those of $Ge_{1-x}Sn_x\{111\}$ shown in Fig. 4(c).

The oblique incident CaF_2 flux direction projected on the sample plane (pole figure) is indicated by the solid arrow in Figs. 4(a)-(c). The locations of three $Ge_{1-x}Sn_x\{111\}$ poles line up with the three {111} poles of CaF_2. When the orientation of {111} poles of $Ge_{1-x}Sn_x$ has the same orientation or 180 rotation orientation with respect to the 111 of the CaF_2, the domains are type A and type B, respectively. The higher intensity in three poles in Fig. 4(c) indicates that $Ge_{1-x}Sn_x$ film has type A domains. The three twin spots from one of the primary poles $(11\bar{1})$ of $Ge_{1-x}Sn_x$ are labeled as $T(\bar{1}1\bar{1})$, $T(1\bar{1}\bar{1})$, and $T(\bar{1}\bar{1}\bar{1})$ as an example in Fig. 4(d). These twin spots are obtained by rotating 180° around the $(11\bar{1})$. If the growth temperature was increased by 50 °C to 350 °C, type

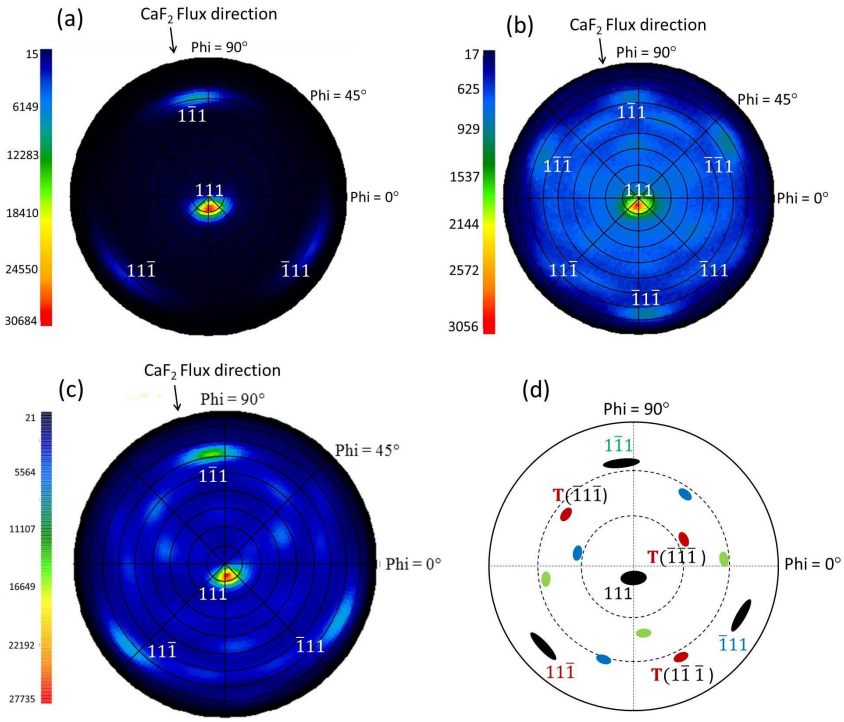

Fig. 4 X-ray 111 pole figures of (a) CaF_2, (b) pure Ge / CaF_2(capping layer + NR) / glass grown at 300 °C and annealed for one hour (c) $Ge_{1-x}Sn_x$/CaF_2(capping layer + NR)/glass grown at 300 °C and annealed for 1 hour, and (d) a schematic of x-ray 111 pole figure of sample in (c).

B domains were observed. For the pure Ge film grown at 400 °C without Sn the type B domains are observed.[16] The density function calculations found that the type B domain most likely results from the bonding of Ge atoms with Ca^{2+} on the CaF_2 surface with the F^- layer depleted.[17] The six low and almost equal intensity poles shown in Fig. 4(b) from the pure Ge sample grown at 300 °C indicate existence of both type A and type B domains.

The out-of-plane and in-plane dispersions of $Ge_{1-x}Sn_x$ at 300 °C growth and annealing temperature can be estimated from the broadened poles as 10.8° ± 0.2° and 14.2° ± 0.7°, respectively. These dispersions are about one degree improvements from those of the 200 °C growth implying an improvement in the preferred orientations at a higher temperature. The amount of dispersion also depends on the dispersion of the starting CaF_2 buffer layer, which in this case is approximately constant. The sample grown at 350 °C does not show further improvement in the pole figure as compared with that of sample grown at 300 °C. The out-of-plane and in-plane dispersions of the film grown at 350 °C are 12.6° ± 0.4° and 14.8° ± 0.6°, respectively. Both dispersions are larger than the corresponding values for the film grown and annealed at 300 °C. From these temperature dependent pole figures we conclude that the sample grown at 300 °C has a better texture quality.

3.3 TEM

3.3.1 ***Energy dispersive x-ray spectrum of $Ge_{1-x}Sn_x$ film:*** Figure 5(a) shows a bright field TEM cross sectional image of the $Ge_{1-x}Sn_x$ film on CaF_2 grown and annealed at 300 °C. The scale bar is 1 μm. There are five distinct regions, CaF_2 nanorods near the bottom of the image, a CaF_2 capping layer (a more continuous layer), a $Ge_{1-x}Sn_x$ film with a rough surface, an ultrathin Au layer, and a Pt coating (sacrificial layer for FIB milling of the sample for TEM). EDS line profile was collected from 20 points. The adjacent points are 40 nm apart. Fig. 5(b) is a plot of CaF_2, Ge and Sn atomic percentages (converted from the weight percentages) from the first 17 points covering about 640 nm of film thickness. The data (points) start from the edge of the CaF_2 substrate, then continue to the interface of CaF_2 and $Ge_{1-x}Sn_x$, the $Ge_{1-x}Sn_x$ film, and end before the dark boundary of Au between $Ge_{1-x}Sn_x$ and Pt. The last three points from Au and Pt are not plotted in Fig. 5(b). Below the $Ge_{1-x}Sn_x$ - CaF_2 interface, the CaF_2 signal dominates (close to 100 % from other scans deep into CaF_2). The CaF_2 decreases to almost zero percent in the $Ge_{1-x}Sn_x$ layer implying that CaF_2 does not diffuse into $Ge_{1-x}Sn_x$ layer. The Ge percentage increases at the interface and reaches over 95 % in the $Ge_{1-x}Sn_x$ film. The Ge concentration in the entire $Ge_{1-x}Sn_x$ film remains nearly

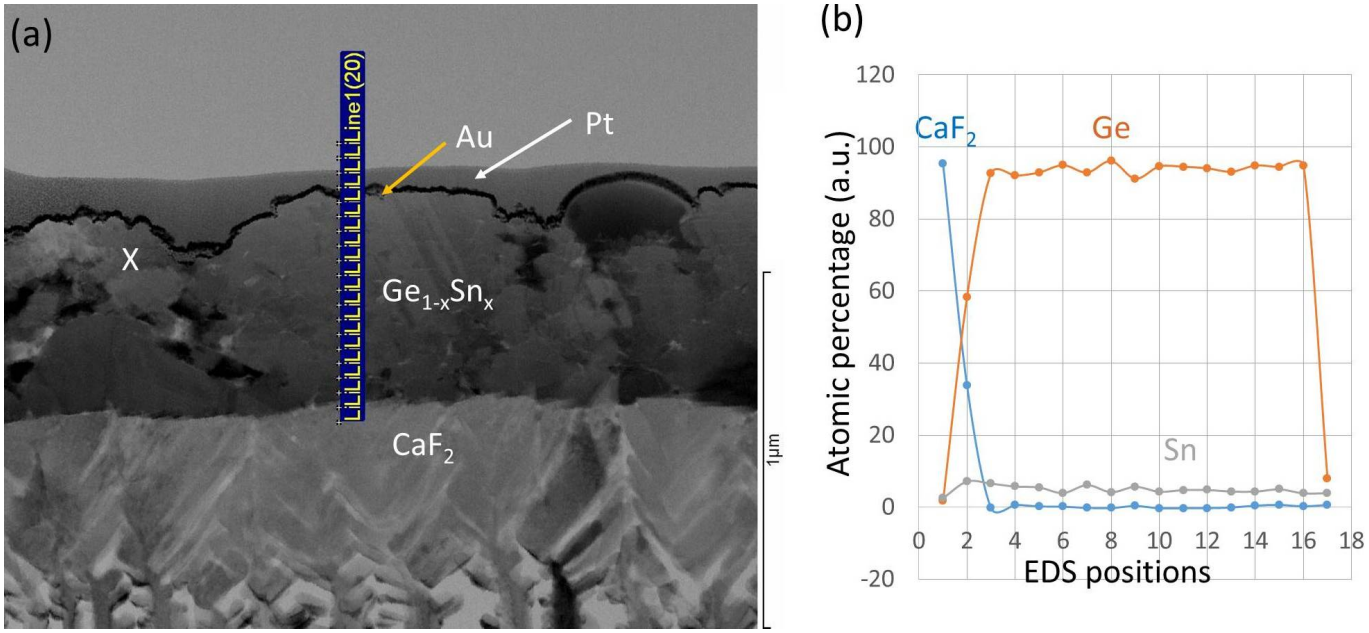

Fig. 5 (a) TEM cross section view of $Ge_{1-x}Sn_x$ / CaF_2(capping layer + NR) / glass grown at 300 °C (b) CaF_2, Ge and Sn concentrations-line profile along the direction perpendicular to the interface and film characterized by EDS.

95 % within the EDS experimental accuracy of ± 1 %. The last data point of Ge near the surface of the $Ge_{1-x}Sn_x$ film (∼ 94 %) is ∼ 2 % more than that the first few data points (∼ 92 %). The highest percentage of Sn is at the $Ge_{1-x}Sn_x$ - CaF_2 interface. The concentration of Sn decreases mildly from ∼ 7 ± 1 % at the interface to ∼ 4 ± 1 % towards the surface of the $Ge_{1-x}Sn_x$ alloy film. The last data point of Sn (∼ 4 %) is ∼ 2 % less than the first few data points (∼ 6 %). Similar EDS composition profiles were obtained from scans across other regions of the interface and $Ge_{1-x}Sn_x$ film. This implies $Ge_{1-x}Sn_x$ is a uniform substitutional alloy film throughout.

3.3.2 ***TEM diffraction pattern and high resolution image of $Ge_{1-x}Sn_x$ film:*** Figure 6(a) shows a TEM diffraction pattern of the $Ge_{1-x}Sn_x$(111) alloy film grown at 300 °C taken from the location marked by "×" in Fig. 5(a). From the symmetry of the diffraction pattern, the zone axis direction is along [011]. A reciprocal unit vector g(111) from 000 to $\bar{1}1\bar{1}$ is labeled as the arrow headed solid line. Other low indices spot like $\bar{2}00$ is also labeled. The ratio of the reciprocal vectors g(200) to g(111) can be estimated from the ratio of the length g(111) from 000 to $\bar{1}1\bar{1}$ to the length g(200) from 000 to $\bar{2}00$. The determined ratio g(200)/g(111) = 1.156. The theoretical ratio for an FCC lattice along the [011] zone axis is 1.155. Thus our indexing of diffraction spots is correct. The conversion of g(200) and g(111) to real space interplanar spacing gives d_{200} = 0.279 nm and d_{111} = 0.320 nm. Considering the accuracy in measuring the reciprocal length, these d spacing values are also consistent with the theoretical calculated real space spacing d_{200} = 0.283 nm and d_{111} = 0.328 nm, respectively. Here we use the lattice constant 0.5688 nm obtained from x-ray diffraction from the sample grown at 300 °C. The diffraction pattern also shows weak twin spots. The twin spots of $\bar{1}1\bar{1}$ and $1\bar{1}1$ are labeled by arrow headed dashed lines. Again the observation of twin spots in TEM diffraction pattern is consistent with the twin poles observed in the x-ray pole figure shown in Fig. 4(c).

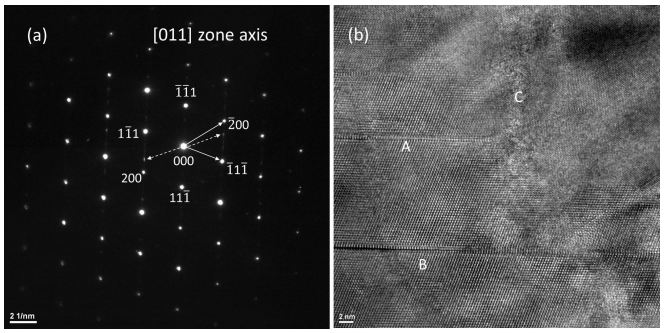

Fig. 6 (a) TEM diffraction pattern of $Ge_{1-x}Sn_x$ along the zone axis of [011] and (b) high resolution TEM image of $Ge_{1-x}Sn_x$ film grown and annealed at 300 °C.

Figure 6(b) shows a typical high resolution TEM image obtained from the location marked by "×" in Fig. 5(a). Single crystal grains can be seen in the viewing area. Single stack-

ing faults (along the horizontal direction) labeled as A and B are seen in a grain. Multiple stacking faults are also seen from other high resolution TEM images. In Fig. 6(b), a grain boundary along the vertical direction of the image labeled C separating two grains can also be seen.

The interface between CaF_2 and $Ge_{1-x}Sn_x$ is rather thick, and a diffraction pattern that covers both $Ge_{1-x}Sn_x$ and CaF_2 cannot be obtained. Diffraction patterns of CaF_2 alone were collected from thin areas of the CaF_2 film. Some diffraction patterns show sharp spots with the symmetry from the $[\bar{1}11]$ zone axis. The conversion of the measured reciprocal vector $g(\bar{2}0\bar{2}) = 5.20$ nm^{-1} from the CaF_2 to real space gives $d_{(\bar{2}0\bar{2})} = 0.192$ nm and is consistent with the theoretically calculated $d_{(\bar{2}0\bar{2})} = 0.193$ nm from CaF_2 with a lattice constant of 0.546 nm. This shows that the structure of CaF_2 buffer layer was not affected by 300 °C growth and annealing temperature. In some areas of the CaF_2, a superposition of diffraction patterns from the [111] zone axis and the [233] zone axis were seen. This indicates there are two CaF_2 crystallites with a relative orientation. This relative orientation can be estimated from the angle between the 111 and 233 planes to be 10 degrees and is consistent with the dispersion angle obtained from the x-ray pole figure shown in Fig. 4(a).

3.4 Raman spectra of $Ge_{1-x}Sn_x$ films

The Sn concentration in $Ge_{1-x}Sn_x$ can be estimated from Raman scattering as a complementary technique to the x-ray diffraction method described in section 3.1.2. Figure 7 shows Raman spectra collected at room temperature from the $Ge_{1-x}Sn_x$ alloy films grown at 200, 250, 300, 350 °C and the pure Ge film grown at 300 °C. The highest peak at 298.00 cm^{-1} is the Ge-Ge vibration mode from pure Ge. This peak is due to longitudinal optical (LO) phonons. We identified three peaks near 290, 260 and 160 cm^{-1} in each spectrum of $Ge_{1-x}Sn_x$ as Ge-Ge [18], Ge-Sn [19], and Sn-Sn vibration modes, respectively. Table 1 lists the peak positions and FWHMs corresponding to each mode with the goodness of fitting parameter R^2 better than 0.99.

We observed several changes associated with these three peaks: (1) The Ge-Ge peak in the $Ge_{1-x}Sn_x$ alloy film shifts from the peak at 298.00 cm^{-1} for pure Ge to 290.54, 291.15, 291.44, and 291.87 cm^{-1} corresponding to the growth temperatures at 200, 250, 300 and 350 °C, respectively. The $\sim$ 7.5 cm^{-1} shift from the pure Ge sample to the $Ge_{1-x}Sn_x$ sample grown at 200 °C gives an estimate of 8 to 9 % Sn concentration in the $Ge_{1-x}Sn_x$ alloy film [20] or $\sim$ 8 to 10 % in another estimate. [18] The small Raman shift of 1.3 cm^{-1} in the Ge-Ge modes between samples grown at 200 and 350 °C is not sensitive to the Sn concentration change. This is unlike x-ray diffraction where a lattice constant change is more sensitive to the Sn concentration change. (2) The Ge-Sn peak shift of $\sim$ 6.15 cm^{-1} from 257.52 to 263.67 cm^{-1} when the growth temperature was changed from 200 °C to 350 °C corresponds to a Sn concentration change from $\sim$ 10 % to $\sim$ 2 % when compared with literature data of Ge-Sn mode frequency in $Ge_{1-x}Sn_x$ alloys. [18] The Sn percentages calculated from the shift of Ge-Sn Raman peak *vs.* growth temperature are listed in Table 1 and plotted in Fig. 3. Due to the broad Raman peak, the maximum peak in each Ge-Sn mode is fitted using a peak fit software (Origin). (3) The Sn-Sn peak shifts about 7.73 cm^{-1} from 160.52 to 168.25 cm^{-1} from samples grown at 200 and 350 °C, respectively. However, there is no literature data to which we can compare the Sn concentration change from the Sn-Sn vibration mode frequency.

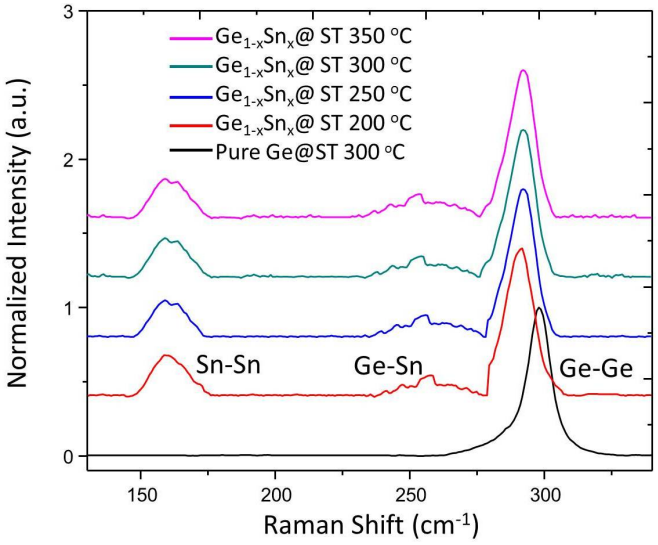

Fig. 7 Raman spectra of pure Ge / CaF_2(capping layer + NR) / glass grown at 300 °C, $Ge_{1-x}Sn_x$ / CaF_2(capping layer + NR) / glass grown at 200, 250, 300 and 350 °C.

The x-ray peak shift shows that the concentration changes from 11.4 % to 3.1 % as the growth temperature increases from 200 °C to 350 °C and is comparable to the concentration change from $\sim$ 10 % to $\sim$ 2 % obtained from the Raman shift observed from Ge-Sn peak. See Fig. 3. We note that in x-ray diffraction the Sn concentration is determined by the micron long probing depth of x-rays that covers the entire $Ge_{1-x}Sn_x$ film thickness (530 $\pm$ 80 nm). In contrast, the laser beam probing depth used in the Raman scattering in Ge is much less, in the range of about 30 nm for a laser of wavelength 532 nm. [21] Thus only the vibrational modes of $Ge_{1-x}Sn_x$ within this probing depth of laser beam contribute to Raman signals. Therefore the Sn concentrations extracted from two techniques differ slightly.

In addition to the shift of Raman peaks as a function of sample growth temperature, the FWHMs of Ge-Ge, Ge-Sn, and Sn-Sn Raman peaks also changed as a function of sam-

Table 1 Raman shifts of Ge-Ge, Ge-Sn and Sn-Sn peaks

Sample growth and annealing temperature	Ge-Ge peak position and peaks FWHM (cm^{-1})	Ge-Sn peak peak position and peaks FWHM (cm^{-1})	Sn-Sn peak peak position and peaks FWHM (cm^{-1})	Sn atomic % estimated from Ge-Sn peaks
Ge-Sn, 200 °C	290.54 ; 12.22	257.52 ; 22.43	160.52 ; 15.87	10 ± 1
Ge-Sn, 250 °C	291.15 ; 12.64	259.14 ; 24.45	161.71 ; 17.26	8 ± 1
Ge-Sn, 300 °C	291.44 ; 11.65	262.15 ; 20.23	163.45 ; 14.35	4 ± 1
Ge-Sn, 350 °C	291.87 ; 11.56	263.67 ; 19.52	168.25 ; 13.57	2 ± 1
Pure Ge	298.00 ; 10.94	N. A.	N. A.	0

ple growth temperature. Recall, lower Sn concentrations for higher growth temperatures. The FWHM increases from 200 °C, reaches a maximum at 250 °C, and then decreases as the growth temperature increases. The width is related to mass change and local bonding configuration among atoms. This variation in FWHM implies that the incorporation of larger size Sn (15 % larger than Ge) and heavier mass Sn (Sn atomic mass 118.71 amu vs Ge atomic mass 72.64 amu) in the Ge lattice introduces a variation in bonding configuration when Sn atoms are substituting in place of Ge atoms. The data show that when the growth temperature is higher than 250 °C, the bonding configuration becomes more uniform (narrower FWHM). One expects the bonding configuration to gradually approach the pure Ge-Ge bonding configuration. However, the FWHM of 11.56 cm^{-1} obtained from the sample grown at the highest growth temperature of 350 °C has not reached the FWHM of 10.94 cm^{-1} associated with the pure Ge film.

The FWHMs of Ge-Sn peaks are about a factor of 1.5 to 2 times wider than those of Ge-Ge and Sn-Sn peaks. This implies that the Ge-Sn bonding configurations have more distortions as compared with pure Ge-Ge or pure Sn-Sn bondings.

3.5 Roughness parameters

Although the structural quality, determined by such factors as the average crystallite size in the vertical direction and in-plane and out-of-plane dispersion, of biaxial $Ge_{1-x}Sn_x$ alloy films improves as the growth temperature increases, the surface morphology still appears very rough, as seen from the TEM cross-section image in Fig. 1(b). Figs. 8(a) and (b) show AFM images of 5 μm × 5 μm areas of the CaF_2 capping layer and $Ge_{1-x}Sn_x$ film grown at 300 °C, respectively. Fig. 8(b) shows 3D island features with lateral sizes of hundreds of nm and a vertical root mean square (RMS) roughness of tens of nm, consistent with the TEM cross-section image. These 3D features are much larger than those of the starting CaF_2 buffer layer. In AFM images collected from all samples, there are protruding islands, which grow larger as the temperature increases. The two-dimensional height-height correlation function, H(r) was analyzed from these AFM images to provide roughness parameters including vertical surface width, ω (or RMS roughness), lateral correlation length, ξ, and roughness exponent, α.[22–24] H(r) is defined as $H(r) = \langle [h(r) - h(0)]^2 \rangle$, where h(r) is the surface height at position r and h(0) is the surface height at a reference position r = 0. Surface width, ω is the square root of $\langle [h(r) - \langle h \rangle]^2 \rangle$, which describes the surface roughness at large distances. The lateral correlation length, ξ describes the wavelength of the surface fluctuations. For self-affine and isotropic surfaces, $H(r) = 2\omega^2[1 - e^{-(r/\xi)^{2\alpha}}]$. For large r, the surface height fluctuations should not be correlated, so $H(r) = 2\omega^2$. For small r, the surface height-height correlation has the asymptotic form $H(r) = (\rho r)^{2\alpha}$, where ρ is a constant and α is the local roughness exponent. α describes how "wiggly" the surface is and has a value ≤ 1, with 1 being the smoothest. These numbers, obtained from H(r), are listed in Table 2.

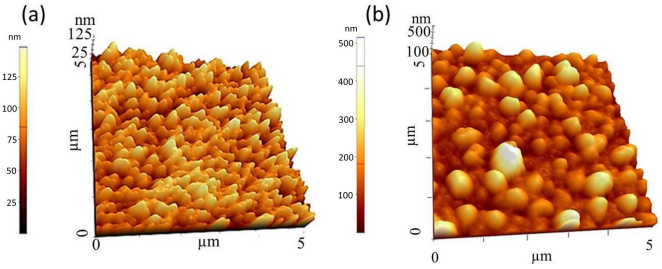

Fig. 8 AFM images (5 μm × 5 μm) of (a) CaF_2 capping layer on CaF_2 nanorods on glass grown at room temperature and (b) $Ge_{1-x}Sn_x$ / CaF_2(capping layer + NR) / glass grown and annealed at 300 °C.

4 Discussions

4.1 Enhancement of Ge diffusion and crystallization by Sn

Based on the results we have obtained, Sn plays a role as a diffusion enhancer for Ge crystallization. The Sn atoms substitute into the Ge lattice to form $Ge_{1-x}Sn_x$ alloy. Literature shows that the monolayer coverage of Sn increases the diffusion length of Ge on Si(111) and the diffusion mobility of Ge atoms on a Si surface by four orders of magnitude.[25] Other work regarding the effect of Sn on Ge growth on Ge(001)

Table 2 Roughness parameters of CaF_2 and $Ge_{1-x}Sn_x$ films analyzed from AFM images

Samples and growth temperature	Surface width ω (nm)	Lateral correlation length ξ (nm)	Local roughness α
CaF_2 (capping layer + NR) room temperature	20.16 ± 0.05	160.00 ± 4.5	0.535
$Ge_{1-x}Sn_x$ room temp. growth and no annealing	30.52 ± 0.16	303.41 ± 8.5	0.697
200 °C annealed $Ge_{1-x}Sn_x$	63.40 ± 0.15	338.62 ± 9.8	0.771
250 °C annealed $Ge_{1-x}Sn_x$	73.70 ± 0.15	397.46 ± 7.2	0.862
300 °C annealed $Ge_{1-x}Sn_x$	78.20 ± 0.26	447.62 ± 17.0	0.878
350 °C annealed $Ge_{1-x}Sn_x$	81.20 ± 0.32	472.74 ± 19.8	0.905

shows that at a low Sn concentration (< 2 %) enhances the Ge diffusion as well as Ge and Sn interlayer mass transport.[26] We believe that Sn has a similar effect on Ge when Ge is deposited on a $CaF_2(111)$ surface. Our x-ray diffraction spectra and x-ray pole figures show that the crystallization of $Ge_{1-x}Sn_x(111)$ films by Sn incorporation starts at 200 °C and the biaxial quality of $Ge_{1-x}Sn_x(111)$ improves at 250 and 300 °C. This is supported by improved out-of-plane and in-plane dispersions, increased average $Ge_{1-x}Sn_x$ grain size in the vertical direction, and a smoother local roughness parameter, α at 300 °C when compared to a pure Ge sample. In contrast, the pole figure of the pure Ge film grown at 300 °C without Sn, as seen in Fig. 4(b), shows very faint poles with pole intensity about one order of magnitude lower than the pole intensity for biaxial $Ge_{1-x}Sn_x(111)$ shown in Fig. 4(c). The x-ray spectrum from the pure Ge film grown at 300 °C without Sn shown in Fig. 2 has a small Ge(111) peak implying a very small amount of crystallization.

4.2 Sn substitution in Ge

From the growth temperature dependent x-ray θ *vs.* 2θ spectra, we did not observe a peak from pure Ge(111) at all temperatures but we observed an obvious Sn(200) peak at room temperature. The Sn(200) peak position stayed at a constant 2θ angle of 30.60° corresponding to the bulk lattice constant of Sn (0.58318 nm), but its peak intensity decreased dramatically and its FWHM increased as the growth temperature increased to 350 °C. The average Sn grain size, derived from the inverse of FWHM, decreases from $\sim$ 52 nm to $\sim$ 9 nm. The reducing intensity and grain size of Sn are partly due to the desorption of Sn at temperatures above its melting point of 232 °C before the Ge deposition. It is also a consequence of the substitution of Sn in the Ge lattice during the formation of $Ge_{1-x}Sn_x$ alloy films. This Sn substitution in the Ge lattice is revealed by the increasing relative peak intensity of the $Ge_{1-x}Sn_x$ Bragg angle as well as the increasing $Ge_{1-x}Sn_x$ grain size as the growth temperature increases.

The observation of high intensity $Ge_{1-x}Sn_x$ peaks and very low intensity Sn peaks implies that under the non-equilibrium growth and annealing conditions the sample can have a mixture of two phases: a dominant alloy film with grains, and small Sn clusters. The Sn clusters could be embedded as the Sn precipitates in the $Ge_{1-x}Sn_x$ film or Sn segregates to the surface of the $Ge_{1-x}Sn_x$ film.[1] The precipitates of beta Sn were observed in $Ge_{1-x}Sn_x$ layers on bulk Ge after post-deposition annealing.[27] For a molecular beam epitaxy grown $Ge_{1-x}Sn_x$ layer on a Ge buffered Si wafer after 620 °C annealing, circular Sn clusters $\sim$ 20 nm in diameter were observed in the $Ge_{1-x}Sn_x$ layer and Sn rich surface layer.[11] In our TEM EDS line scan, the Sn concentration in CaF_2 is negligible and the concentration is the highest at the interface between CaF_2 and $Ge_{1-x}Sn_x$ (where Sn was deposited) and decreases to a nearly constant concentration of less than 5 % in the $Ge_{1-x}Sn_x$ film. If there exist small Sn clusters of size $<$ 10 nm, the 40 nm adjacent EDS probing separation would not be able to reveal it. However, the EDS has a couple of locations such as data points 7 and 9 that have slightly larger Sn concentrations. This is not inconsistent with the existence of very small Sn clusters inferred from the low intensity x-ray peak and its broad FWHM.

4.3 Raman peak shifts and composition change

The Ge-Ge Raman peak position measured from our pure Ge film grown at 300 °C is 298 cm^{-1}. This peak from the $Ge_{1-x}Sn_x$ alloy film grown at 200 °C is 290.34 cm^{-1}, about a 7.5 cm^{-1} deviation from that of the pure Ge film. Because Raman scattering is sensitive to crystal potential fluctuations and change in local atomic bonding arrangement, we can infer that this $\sim$ 7.5 cm^{-1} shift indicates that the substitutional Sn changes local atomic arrangement. For dilute $Ge_{1-x}Sn_x$ alloy films, or those with a low percentage of Sn, the local atomic arrangement is similar. When the growth temperature increases from 200 to 350 °C, the shift of the Ge-Ge peak in the $Ge_{1-x}Sn_x$ films is much less, within about 1.3 cm^{-1}. Recent theoretical calculations of the Raman shift in Ge nanowires indicate that a dramatic Raman shift in the Ge-Ge peak from 300 cm^{-1} to 290 cm^{-1} occurs for a nanowire cross-section of $\sim$ 2 nm.[28] Experimental results of Raman peaks measured from Ge nanowires as a function of cross-sectional diameter show almost constant Raman peaks with no Raman shift between wire diameters of 20 and 100 nm. Only when the wire diameter was reduced to about 5 nm, was a 3 cm^{-1} Raman shift of

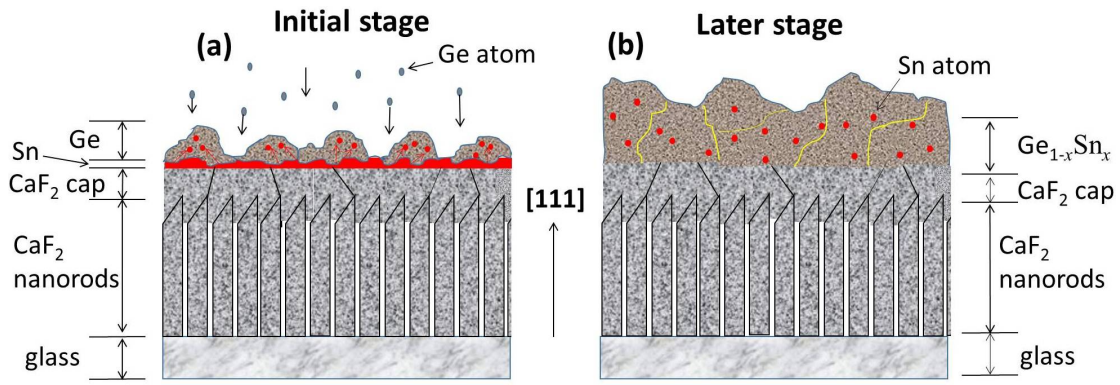

Fig. 9 Schematics (not to scale) of (a) early stage and (b) later stage of Ge deposition on biaxial Sn / CaF_2(capping layer + NR) / glass substrate at an elevated growth temperature. The blue dots, red dots and red layer in (a) represent Ge atoms, Sn atoms (diffusing into the Ge layer), and the mobile Sn layer, respectively. The red dots in (a) and (b) represent substitutional Sn atoms (its size is highly exaggerated) in the Ge lattice. The black and yellow curves in (a) and (b) represent boundaries in the CaF_2 capping layer and Ge layer, respectively.

the Ge-Ge peak observed.[29] From our x-ray diffraction study we learned that the average grain size of $Ge_{1-x}Sn_x$ films increases from $\sim$ 50 nm at a 200 °C growth temperature to $\sim$ 63 nm at 350 °C. In this size range (several tens nm) the Raman Ge-Ge peak should not have a shift from the size effect that occurs at about 5 nm. The fact that a Raman shift in the Ge-Ge mode was observed in the $Ge_{1-x}Sn_x$ film must then be due to the substitutional Sn within the film. The Raman shift can be modeled as the sum of a mass term (due to the difference between the masses of Ge and Sn) and a bond term (due to near neighbor bond distortions) in an alloy.[18] The first few percent of Sn substitution in $Ge_{1-x}Sn_x$ film cause the 7.5 cm^{-1} Raman shift of the Ge-Ge peak from the pure Ge film. However, for a few percent Sn concentration in $Ge_{1-x}Sn_x$ film, the local environment of the Ge-Ge bond is similar and is not sensitive to a few percent change of Sn concentration. This is reflected in the small Ge-Ge Raman peak shift of only 1.3 cm^{-1} from samples grown at 200 °C to those grown at 350 °C.

In contrast, the Raman shifts in Ge-Sn peaks are more sensitive to variation of Sn concentration because of the Ge-Sn bonding. This is reflected in the larger 6.15 cm^{-1} Raman peak shift 1 from samples grown at 200 °C to those grown at 350 °C. This more sensitive shift among samples grown at different temperatures allows Sn concentration to be estimated from literature data of Ge-Sn mode frequency in $Ge_{1-x}Sn_x$ alloys.[18] The quantitative relationship between Sn concentration and growth temperature is consistent with the x-ray results shown in Fig. 3.

4.4 Temperature dependent growth of morphological feature size and grain size

As growth temperature increases, the surface width (RMS roughness), lateral correlation length, and local roughness exponent increase. If we take the ratio of lateral correlation length to surface width from Table 2, we find these ratios are $\sim$ 5.34, $\sim$ 5.38, $\sim$ 5.71, and $\sim$ 5.81, for growth temperatures of 200, 250, 300 and 350 °C, respectively. This implies that although the surface features appear rough, the lateral growth rate is still larger than the vertical growth rate. In addition, values for the local roughness exponent, α increase from 0.77 to 0.90. A local roughness value of 1 implies a less rugged local slope. This increase α value implies a less rugged local surface for higher growth temperatures, which is consistent with the increasing ratio of lateral size to vertical roughness.[22–24]

This rough surface is expected from the surface energy differences in different materials. Surface energies of Ge[30], Sn[31] and $CaF_2(111)$[32] are 1.06 J/m^2, 0.795 J/m^2, and 0.45 J/m^2, respectively. It is expected that Sn will grow on CaF_2 as Volmer Weber (VW) 3D islands and that Ge will follow 3D island growth on Sn. Literature reports that kinetic roughening occurs during the $Ge_{1-x}Sn_x$ growth on Ge buffered Si(100) substrates[10] as well as on Ge(001) surfaces.[26]

From Table 2 the $\sim$ 450 nm lateral correlation length of the $Ge_{1-x}Sn_x$ film grown at 300 °C is a few times larger than $\sim$ 60 nm average vertical grain size of $Ge_{1-x}Sn_x$ obtained from XRD in section 3.1.3. This means each morphological island contains a few crystalline grains. The cross-section TEM image (Fig. 5(a)) shows many morphological features hundreds of nm in diameter (the 1 μm scale bar is on the right margin of Fig. 5(a)), consistent with AFM images. The high resolution TEM image (Fig. 6(b)) shows grain boundaries with an average grain size (71 $\pm$ 9 nm) of the same order of magnitude as that obtained from the FWHM of the x-ray peak profile. The boundaries among the grains may serve as pathways for Ge diffusion to form crystallites.[33,34] The increasing surface correlation length and the average grain size as the growth temperature increases are the results of possible liquid-

like Sn at Sn melting temperature of 232 °C and above. The liquid state of Sn enhances Ge diffusion and the crystallization of $Ge_{1-x}Sn_x$ films as compared with solid-like Sn below 232 °C. These conclusions are supported by the results of x-ray diffraction (section 3.1.3) and AFM (Table 2).

5 Summary and conclusion

Based on the above results and discussions, we summarize the $Ge_{1-x}Sn_x(111)$ formation process schematically in Fig. 9 (not to scale) from the early to later stages of Ge deposition on the biaxial Sn / CaF_2(capping layer + NR)/glass substrate at an elevated growth temperature. The Sn atoms in the Sn layer at the $CaF_2(111)$ surface diffuse into the condensing Ge layer being deposited. They substitute in place of Ge atoms within the Ge lattice and induce crystallization of the $Ge_{1-x}Sn_x$ film at temperatures as low as 200 °C. The concentration of Sn in the $Ge_{1-x}Sn_x(111)$ film was shown to depend on the growth temperature. The surface of the crystallized $Ge_{1-x}Sn_x(111)$ film is morphologically rough and has finite-sized grains with stacking faults and grain boundaries.

We demonstrated that biaxial $Ge_{1-x}Sn_x(111)$ alloy films containing a few percent of Sn can be grown on amorphous glass substrates by first depositing a biaxial $CaF_2(111)$ buffer layer on glass. The x-ray diffraction, x-ray pole figure and TEM diffraction show the best $Ge_{1-x}Sn_x(111)$ film was grown at 300 °C, much lower than pure Ge crystallization temperature (over 600 °C)[35] or pure Ge grown on CaF_2 capping layer on CaF_2 nanorods without Sn ($\sim$ 400 °C). The epitaxy relationships obtained from the x-ray pole figures are $Ge_{1-x}Sn_x\langle\bar{1}01\rangle \parallel CaF_2\langle\bar{1}01\rangle$ and $Ge_{1-x}Sn_x\langle\bar{1}10\rangle \parallel CaF_2\langle\bar{1}10\rangle$. The lattice constants obtained from x-ray diffraction of the $Ge_{1-x}Sn_x(111)$ film provides Sn concentrations and are consistent with TEM EDS results. The EDS shows that Sn is uniformly distributed throughout the $Ge_{1-x}Sn_x(111)$ film and that no Ca diffuses into the $Ge_{1-x}Sn_x(111)$ film. Raman shift from the Ge-Sn peak is sensitive to the Sn concentration change and supports the concentration obtained from x-ray diffraction. The morphological feature size determined by AFM is about 450 nm, each containing many grains of about 60 nm in diameter, as determined by x-ray diffraction and high resolution TEM images. The lattice constant of the $Ge_{1-x}Sn_x(111)$ alloy film grown at 300 °C is within 0.5 % of a pure Ge (111) film. This growth method may be applicable to other alloy materials that have low eutectic points.

Acknowledgement

This work is supported by NSF DMR-1104786, New York State Foundation of Science, Technology and Innovation (NYSTAR) through Focus Center-New York, and Rensselaer. TEM study was carried out in whole at the Center for Functional Nanomaterials, Brookhaven National Laboratory, which is operated by the U.S. department of Energy, Office of Basic Sciences, under contract no. DE-AC02-98CH10886. We thank Aaron Littlejohn for comments and editing.

References

1 E. Kasper, J. Werner, M. Oehme, S. Escoubas, N. Burle and J. Schulze, *Thin Solid Films*, 2012, **520**, 3195–3200.
2 H. P. L. de Guevara, A. G. Rodriguez, H. Navarro-Contreras and M. A. Vidal, *Appl. Phys. Lett.*, 2004, **84**, 4532–4534.
3 N. Bhargava, M. Coppinger, J. P. Gupta, L. Wielunski and J. Kolodzey, *Appl. Phys. Lett.*, 2013, **103**, 041908.
4 M. Coppinger, J. Hart, N. Bhargava, S. Kim, and J. Kolodzey, *Appl. Phys. Lett.*, 2013, **102**, 141101.
5 M. Oehme, M. Schmid, M. Kaschel, M. Gollhofer, D. Widmann, E. Kasper, and J. Schulze, *Appl. Phys. Lett.*, 2012, **101**, 141110.
6 S. Su, W. Wang, B. Cheng, G. Zhang, W. Hu, C. Xue, Y. Zuo and Q. Wang, *Journal of Crystal Growth*, 2011, **317**, 43–46.
7 H. P. L. de Guevara, A. Rodriguez, H. Navarro-Contreras and M. A. Vidal, *Appl. Phys. Lett.*, 2003, **83**, 4942.
8 C. S. Cook, S. Zoller, M. R. Bauer, P. Aella, J. Kouvetakis and J. Menendez, *Thin Solid Films*, 2004, **455–456**, 217–221.
9 M. Bauer, J. Taraci, J. Tolle, A. V. G. Chizmeshya, S. Zollner, D. J. Smith, J. Menendez, C. Hu and J. Kouvetakis, *Appl. Phys. Lett.*, 2002, **81**, 2992.
10 S. Su, W. Wang, B. Cheng, W. Hu, G. Zhang, C. Xue, Y. Zuo and Q. Wang, *Solid State Communications*, 2011, **151**, 647–650.
11 H. Li, Y. X. Cui, K. Y. Wu, W. K. Tseng, H. H. Cheng and H. Chen, *Appl. Phys. Lett.*, 2013, **102**, 251907.
12 Y. Kinoshita, R. Matsumura, T. Sadoh, T. Nishimura and M. Miyao, *ECS Transactions*, 2013, **58**, 179–184.
13 H.-F. Li, T. Parker, F. Tang, G.-C. Wang, T.-M. Lu and S. Lee, *Journal of Crystal Growth*, 2008, **310**, 3610–3614.
14 C. Gaire, P. Snow, T.-L. Chan, W. Yuan, M. Riley, Y. Liu, S. B. Zhang, G.-C. Wang and T.-M. Lu, *Nanotechnology*, 2010, **21**, 445701.
15 M.-H. Lee, P.-L. Liu, Y.-A. Hong, Y.-T. Chou, J.-Y. Hong and Y.-J. Siao, *J. Appl. Phys.*, 2013, **113**, 063517.
16 C. Gaire, P. C. Clemmer, H.-F. Li, T.-C. Parker, P. Snow, I. Bhat, S. Lee, G.-C. Wang and T.-M. Lu, *Journal of Crystal Growth*, 2010, **312**, 607–610.
17 T.-L. Chan, C. Gaire, T.-M. Lu, G.-C. Wang and S. B. Zhang, *Surface Science*, 2010, **604**, 1645–1648.
18 V. R. D'Costa, J. Tolle, R. Roucka, C. D. Poweleit, J. Kouvetakis and J. Menendez, *Solid State Communications*, 2007, **144**, 240–244.
19 R. Schorer, W. Wegscheider and G. Abstreiter, *J. Vac. Sci Technol. B*, 1993, **11**, 1069.
20 H. Lin, R. Chen, Y. Huo, T. I. Kamins and J. S. Harris, *Appl. Phys. Lett.*, 2011, **98**, 261917.
21 M. Moreau and G. L. Bourdon, *http://www-origin.horiba.com /fileadmin/uploads/Scientific/Documents/Raman/spring05.pdf*.
22 S. K. Sinha, E. B. Sirota and S. Garoff, *Phys. Rev. B*, 1988, **38**, 2297.
23 T.-M. Lu, H.-N. Yang, and G.-C. Wang, *Mat. Res. Soc. Symp. Proc.*, 1995, **367**, 283.
24 Y.-P. Zhao, G.-C. Wang and T.-M. Lu, *Characterization of amorphous and crystalline rough surface: principles and applications*, Academic Press, (Experimental Methods in the Physical Science Vol. 37), 6th edn., 2001.
25 A. E. Dolbak and B. Z. Olshanetsky, *Cent. Eur. J. Phys*, 2008, **6**, 634–637.
26 K. A. Bratland, T. S. Y. L. Foo and, H.-S. Seo, R. T. Seo, R. T. Haasch, P. Desjardins and J. E. Greene, *J. Appl. Phys.*, 2005, **97**, 044904.

27 S. Takeuchi, A. Sakai, O. Nakatsuka, M. Ogawa and S. Zaima, *Thin Solid Films*, 2008, **517**, 159–162.
28 P. Alfaro-Calderon, M. Crus-Irisson and C. Wang-Chen, *Nanoscale Res. Lett.*, 2008, **3**, 55–59.
29 X. Wang, A. Shakouri, B. Xu, S. Su and M. Meyyappan, *J. Appl. Phys.*, 2007, **102**, 014304.
30 J. Wollschlager, D. D, C. R. Wang, B. H. Muller and K. R. Hofmann, *J. Appl. Phys.*, 2011, **110**, 102205.
31 M. S. Sellers, A. J. Schultz, C. Basaran and D. A. Kofke, *Appl. Surf. Sci.*, 2010, **256**, 4402–4407.
32 V. E. Puchin, A. V. Puchina, M. Huisinga and M. Reichhling, *J. Phys.: Condens. Matter*, 2001, **13**, 2081–2094.
33 S. Ingrey and B. MacLaurin, *J. Vac. Technol. A*, 1984, **2**, 358.
34 W. J. Edwards, H. Tsutsu, D. G. Ast and T. I. Kamins, *MRS Proceedings*, 1993, **319**, 183.
35 Z. H. Cao, P. Liu, X. K. Meng, S. C. Tang and H. M. Lu, *Appl. Phys. A*, 2009, **94**, 393–398.